CRYSTAL GROWTH & DESIGN

Article

Cite This: Cryst. Growth Des. 2018, 18, 7275−7285

pubs.acs.org/crystal

Salt Recovery from Wastewater Using Membrane Distillation−Crystallization

I. Ruiz Salmón,* K. Simon, C. Clérin, and P. Luis

Materials & Process Engineering (iMMC-IMAP), Université Catholique de Louvain, Place Sainte Barbe 2, 1348 Louvain-la-Neuve, Belgium

Supporting Information

ABSTRACT: Osmotic membrane distillation−crystallization is proposed in this study to recover sodium carbonate, potassium nitrate, and sodium sulfate from synthetic industrial solutions leading to valorization of the salts of wastewater coming from gas treatment (flue gases containing CO_2, SO_2, or NO_x) or from brines. The technical viability of the process is discussed in terms of transmembrane fluxes, mass transfer coefficients, and the crystal purity. The effect of concentrations of the feed and osmotic solution, flow rates, and presence of impurities (traces of different salts) was determined as well. The osmotic concentration was the main parameter affecting the transmembrane flux. The concentration of the three salts in the feed had a slight influence, and no effect could be observed by the study of flow rates. Constant mass transfer coefficients were obtained. Two membrane contactors in series were connected to increase the membrane area in order to technically validate one of the main advantages of this kind of technology: the linear and easy scale-up. Super high-purity crystals were produced: $Na_2CO_3{\cdot}10H_2O$, $Na_2SO_4{\cdot}10H_2O$, and KNO_3 free-of-impurity crystals (no Cl^- and salt traces trapped), ready to be reused in the industry, if desired. No cocrystallization was observed, which is a remarkable difference with conventional crystallization systems (evaporators), a partial amorphous structure is detected by X-ray diffraction, and fairly pure, large crystals were obtained.

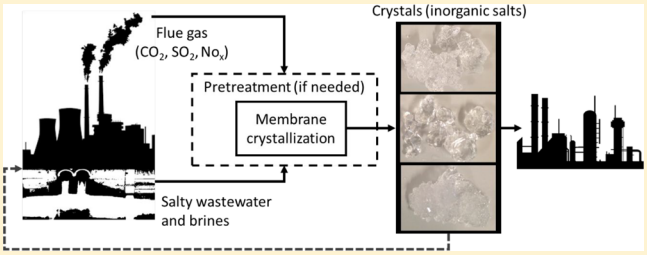

1. INTRODUCTION

Brines and salty wastewater may strongly affect the environment if its disposal is not properly carried out. The presence of inorganic soluble salts in water causes osmotic stress for aquatic life at the cellular level, which impacts, for example, the growth of micro-organisms.[1] Besides, high concentrations of inorganic nutrients, such as phosphates, nitrates, or sulfates, may lead to a dangerous phenomenon called eutrophication, characterized by an unusual growth of plants and algae, with important consequences on the composition, structure, and dynamics of the ecosystem. If this happens, the load of organic matter (typically of a single species of algae) may cause the intoxication of fauna, and the turbidity will prevent light from penetrating to the bottom of the ecosystem, and therefore, oxygen production becomes limited.[2] Furthermore, turbidity in water (e.g., caused by high concentrations of calcium carbonate) is frequently used as a quality indicator to assess its compatibility in applications where aquatic organisms exist and even may cause a constraint on predator−prey interactions in those environments.[3]

Current brine and salty wastewater treatments, such as ion exchange[4,5] or membrane filtration by means of reverse osmosis[6] or nanofiltration,[7] are mainly focused on water reuse by eliminating the inorganic salts. A step forward in this objective is a zero discharge process[8] in which the residual stream is separated into two currents: the solvent and the salt to be reused. Salts recovered from wastewater can be used in multiple industrial applications (fertilizers, detergents, ceramics, cement, metallurgical, or petrochemical industry), and its valorization may suppose not only the compliance of legal eco-requirements but also the possibility to produce and sell inorganic salts competing with traditional processes.[9]

Salty wastewater often has heterogeneous compositions with a predominant component, such as the residual streams coming for the treatment of flue gases with alkaline solvents. In the case of CO_2 capture, the flue gas usually contains other compounds, such as SO_2 or NO_x. The reaction of these gases with NaOH may produce, therefore, carbonates[10] and smaller amounts of sulfates[11] or nitrates.[12] If the objective is the capture of SO_2 or NO_x instead of CO_2, the reaction with NaOH will produce aqueous solutions with a high amount of sulfates or nitrates, respectively. For instance, SO_2 is widely emitted in the production of sulfuric acid and nonferrous metals,[13] and the NO_x is the main compound in the emissions of the manufacture of sodium nitrite.[12] Besides the gas treatment, residual aqueous solutions can directly come from industrial wastewater to be recovered, such as the sodium sulfate streams in Solvay production.[14] Therefore, the

Received: April 17, 2018
Revised: October 22, 2018
Published: October 29, 2018

DOI: 10.1021/acs.cgd.8b00580
Cryst. Growth Des. 2018, 18, 7275−7285

predominant compound in the inorganic mixture to be valorized may vary depending on the origin of the stream (kind of process and industry, with or without pretreatment, etc.).

In this context, conventional crystallization using evaporators or crystallizers to separate and/or purify crystalline solid products has been the most extended technology. However, major disadvantages are the large amount of energy needed and the unknowns still existing about the crystallization kinetics, the effect of additives, and the modeling and prediction of polymorphs mechanism.[15] Crystallization has experienced a technological evolution from the conventional operation to a high-efficiency process. Currently, the interest in membrane crystallization is exponentially growing—more than a third of the research publications on crystallization processes is now focused on membrane distillation and membrane crystallization.[16] This technique aims at reaching the production or the recovery of crystals by means of membrane technology, concretely membrane contactors. Easy scale-up and low energy consumption are two of the main advantages of this technology.[17] Membrane distillation−crystallization works properly at room temperature, although residual energy could be used to enhance the transmembrane flux, typically running with temperatures lower than 50 °C.[18] On the other hand, conventional evaporators involve the use of high temperatures to heat the crystallizing solutions and to vaporize the solvent; in conventional crystallizers, solutions are cooled to decreased the solubility of the solute.

Crystal purity is also influenced by the fluid-dynamics of the process. Scaling-up conventional equipment, such as batch stirred tanks, usually involves a change in the hydrodynamics of the system. An important shear stress and limitations in working under continuous mode have been identified.[17] On the contrary, membrane crystallization usually works in a laminar regime independently of the scale, and, therefore, good crystalline structures can be obtained. Besides, the high porosity of the membrane and the large membrane surface can favor crystal nucleation. Membrane distillation−crystallization is a novel technology that can lead to high-purity crystals.[19]

Membrane distillation is commonly used to perform crystallization.[20,21] It is typically used for concentrating solutions, but if the process continues up to the saturation, the solute will precipitate in a crystalline way. Membrane contactors are the common device in which membrane distillation−crystallization is performed. Here, a nondispersive contact is produced thanks to the membrane, which acts as a separation barrier (without providing selectivity) between two phases. The hydrophobic character of the porous membrane allows the contact between both phases without mixing and minimizing membrane wetting. If a highly concentrated (osmotic) solution is used at the permeate side, the process is known as osmotic membrane distillation. The difference of water activity at both sides of the membrane leads to a driving force that causes the water transfer. Water permeates thus from the feed through the membrane due to the gradient of partial pressures between both sides. If water permeation continues over time until the supersaturation of the feed solution, crystallization will then occur. Besides, the membrane provides an excellent support for heterogeneous nucleation, easier than the homogeneous one.[18] Previous works have shown the potential of this technology for sodium carbonate and sodium sulfate crystallization in the context of capture of CO_2 and SO_2 from flue gases.[22−25]

In this work, a rigorous study of synthetic salt aqueous solutions of Na_2CO_3, Na_2SO_4, and KNO_3 has been performed using osmotic membrane distillation−crystallization aiming to crystallize the salts. The influence of concentrations, flow rates, and impurities were studied in order to demonstrate the potential of this technique to recover valuable salts from wastewater.

2. EXPERIMENTAL SECTION

2.1. Chemicals. Na_2CO_3 (anhydrous, AnalaRNormapur, 99.5%), Na_2SO_4 (anhydrous, AnalaRNormapur, 99.5%), and KNO_3 (anhydrous, AnalaRNormapur, 99.5%) were used to prepare the synthetic wastewater coming from industrial production. NaCl (anhydrous, AnalaRNormapur, 99.5%) was used to prepare the osmotic solution that generates the driving force. Deionized water (18.2 MΩ cm^{-1}) was used to prepare all solutions.

2.2. Experimental Methodology. The osmotic membrane distillation−crystallization setup used in this work is shown in Figure 1. Both feed and osmotic streams run in counter-current mode in the hollow fiber membrane contactor (2.5 × 8 Extra-Flow ModuleLiqui-Cel, Membrana GmbH, Germany). The characteristics of the membrane contactor are shown in Table 1.

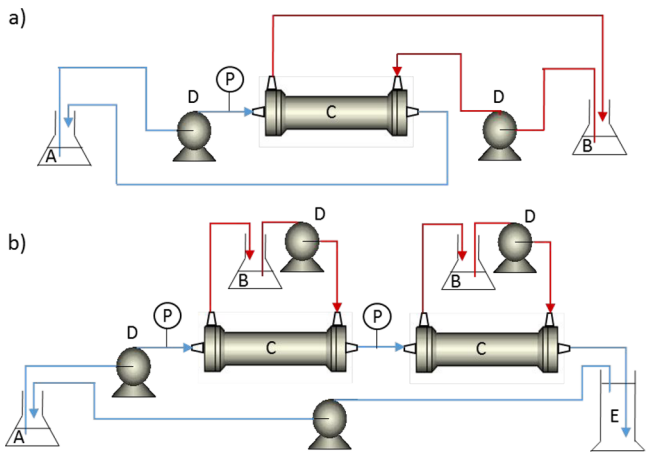

Figure 1. Osmotic membrane distillation−crystallization setup: (a) one contactor, (b) two contactors in series. A, feed solution; B, osmotic solution; C, membrane contactor; D, pumps; P; pressure control system; E, reservoir for crystal growth.

This specific contactor was selected due to (i) the material—polypropylene—which allows the mass transfer without any kind of reaction with the inorganic media at both sides of the membrane; (ii)

Table 1. Characteristics of the Hollow Fiber Contactor

parameters	data from manufacturer
module configuration	hollow fibers
membrane/potting material	polypropylene/polyethylene
fiber i.d./o.d. (μm)	240/300
wall thickness (μm)	40
effective pore size (μm)	0.04
porosity (%)	40
effective fiber length (m)	0.16
effective membrane surface area (m^2)	1.4
number of fibers	10200
burst strength (bar)	27
contact angle (deg)	112

DOI: 10.1021/acs.cgd.8b00580
Cryst. Growth Des. 2018, 18, 7275−7285

Table 2. Experimental Conditions Used in This Work for Membrane Characterization

	feed solution		osmotic solution	
	concentration (g L^{-1})	flow rates (mL min^{-1})	concentration (g L^{-1})	flow rates (mL min^{-1})
one contactor (Na_2CO_3)	10−150	300	200−300	450
one contactor (Na_2SO_4)	20−170	300−400	200−300	300−811
one contactor (KNO_3)	10−250	300−410	200−300	450−810
two contactors (Na_2CO_3)	150	300	300	450

the hydrophobicity of the membrane, which should prevent the aqueous phases from penetrating into the pores; (iii) the large area per volume; (iv) the opportunity to work in cocurrent or counter-current mode and easily placing the contactors in series; (i) the possibility to compare the results with previous works where a smaller contactor but the same membrane characteristics were used. The selected configuration (hollow fibers) leads to a very compact system with a specific surface area of 1077 m^2/m^3, approximately, and a large porosity (40%), which favors the heterogeneous crystallization, easier than the homogeneous one.

In Figure 1a, the feed solution (i.e., aqueous solution of pure Na_2CO_3, Na_2SO_4, KNO_3, or mixtures) was pumped to the membrane through the lumen side (inside of the hollow fibers) of the membrane. Clogging is a critical issue in membrane crystallization that has to be controlled since it would lead to operating problems or even membrane damage. Introducing the feed solution in the lumen side seems the best option since the mass transfer resistance is typically smaller than that produced in the shell side. Thus, local super-saturation could be minimized. Meanwhile, the osmotic stream (NaCl) circulated in counter-current mode through the shell side (outside of the hollow fibers). Both streams, the feed and the osmotic streams, were recirculated to their respective reservoirs. The influence of concentrations of the feed and osmotic solutions as well as the flow rates on the transmembrane flux was studied. A second experimental setup consisting of two membrane contactors placed in series was used in order to increase the membrane area (Figure 1b). The outlet of the first membrane contactor is the feed of the second one; the outlet of the second contactor is sent to a reservoir to allow the growth of the crystals. The overnatant liquid is recycled to the fist reservoir. Regarding the osmotic side, two different solutions were used, one for each membrane contactor. Table 2 shows the experimental conditions for both systems. It is particularly important to measure and control the pressure at the inlet of the membrane contactor ("P" in Figure 1) to prevent blockage by scaling.

The transmembrane flux (J, $m^3\ m^{-2}\ s^{-1}$) was calculated according to eq 1, by means of experimentally weighting of the feed reservoir over time.

$$J(t_i) = -\frac{1}{A}\frac{dV_p}{dt} \approx -\frac{1}{A\rho_{water}}\frac{dw_f}{dt} = -\frac{1}{A\rho_{water}}\frac{w_f(t_{i+1}) - w_f(t_i)}{t_{i+1} - t_i} \quad (1)$$

where V_p (m^3) is the volume of water permeated from the feed solution to the osmotic solution; A (m^2) is the membrane area, ρ_{water} (kg m^{-3}) is the density of water; w_f (kg) is the weight of the reservoir containing the feed solution at time t_i (s).

The transmembrane flux is affected by the driving force; this is the partial pressure and water activities of both feed and osmotic solution. In order to eliminate the effect of the driving force, the overall mass transfer coefficient, K_{ov} (m $Pa^{-1}\ s^{-1}$) is calculated as follows:[22,23]

$$K_{ov} = \frac{J}{(p_f^* a_f - p_p^* a_p)} \quad (2)$$

This coefficient allows evaluating the real membrane performance.[26] In eq 2, J is the experimental water flux calculated with eq 1, and a (−) and p^* (Pa) represent the water activity[27] and the vapor pressure of the feed (f) and the osmotic (p) side, respectively. The vapor pressure is directly related with the salt concentration of the solution. Regarding the conditions of the NaCl, Na_2CO_3, Na_2SO_4, and KNO_3 solutions, the mole fraction of the solvent ranged from 0.92 to 0.94, 0.98 to 0.99, 0.97 to 0.99, and 0.96 to 0.99, respectively, close to unity; i.e., the pure water vapor pressure. Therefore, it is assumed the pure water vapor pressure for calculations leading to simplify them.

Water activities for the four salts involved in the process are plotted in Figure S1 (Supporting Information). The system ran at room temperature (20 ± 1 °C).

2.3. Analytical Methods. *2.3.1. Total Water Fraction (TWF).* The content of water in the crystal was analyzed in order to know which hydrate form is produced. This method starts taking the crystals dried; i.e., the remaining water present on the crystals surface coming from the filtration process is previously dried with a soft tissue. Next, crystals are placed on a chamber for a period of 24 h and finally introduced in an oven at 105 °C for 4 h leading to remove the water contained in the structure.

The water fraction is then defined as a ratio given by the weight of the empty platter ($W_{platter}$), the weight of the platter with crystals before the 24 h in the chamber ($W_{initial}$) and after the oven treatment ($W_{105°C;4h}$):

$$TWF = \frac{w_{initial} - w_{105°C;4h}}{w_{initial} - w_{platter}} \quad (3)$$

Table 3 shows the theoretical water fraction for the different forms of each salt. The solubility curves for the three salts can be found in Figures S2−S4 (Supporting Information).

Table 3. Theoretical Water Content for Different Crystals

crystal	$TWF_{theoretical}$ (wt %)
KNO_3	0
Na_2CO_3	0
$Na_2CO_3{\cdot}H_2O$	14.53
$Na_2CO_3{\cdot}7H_2O$	54.33
$Na_2CO_3{\cdot}10H_2O$	62.96
Na_2SO_4	0
$Na_2SO_4{\cdot}7H_2O$	47.03
$Na_2SO_4{\cdot}10H_2O$	55.91

2.3.2. Charpentier−Volhard's Method. The composition of feed solutions only have pure salts or a mixture of the salts. In osmotic membrane distillation, water should only permeate from the feed side to the osmotic side in vapor phase. However, if membrane wetting takes place, some Cl^- or Na^+ ions coming from the osmotic NaCl solution could cross the membrane to the feed. Previous research by Luis et al. (2013)[25] demonstrated that this phenomenon may occur. Detecting those ions in solution is an indication of membrane wetting.

The Charpentier−Volhard's method is typically used to determine the amount of Cl^-, and it has been used for characterizing both the feed solution and the obtained crystals once the experiments had finished. It is a back-titration method where all the Cl^- precipitates as AgCl by adding $AgNO_3$ in excess according to reaction R1. Then, precipitates are withdrawn from solution, and a second titration is made to measure the amount of Ag^+ employed by adding KSCN (reaction R2). Finally, an indicator containing Fe^{3+} ends the method when the solution becomes dark red (no more Ag^+ ions present). The number of moles of Cl^- present is given by eq 4:

$$Ag^+_{(aq)} + Cl^-_{(aq)} \rightarrow AgCl_{(s)} \quad (R1)$$

DOI: 10.1021/acs.cgd.8b00580
Cryst. Growth Des. 2018, 18, 7275−7285

Table 4. Composition of the Mixtures Crystallized

salt	Mixture 1	Mixture 2	Mixture 3	Mixture 4	Mixture 5	Mixture 6
Na_2CO_3 (wt %)	98.02	95.36	1.39	2.31	1.42	0.00
KNO_3 (wt %)	1.98	1.93	96.75	2.21	98.58	2.26
Na_2SO_4 (wt %)	0.00	2.71	1.86	95.48	0.00	97.74

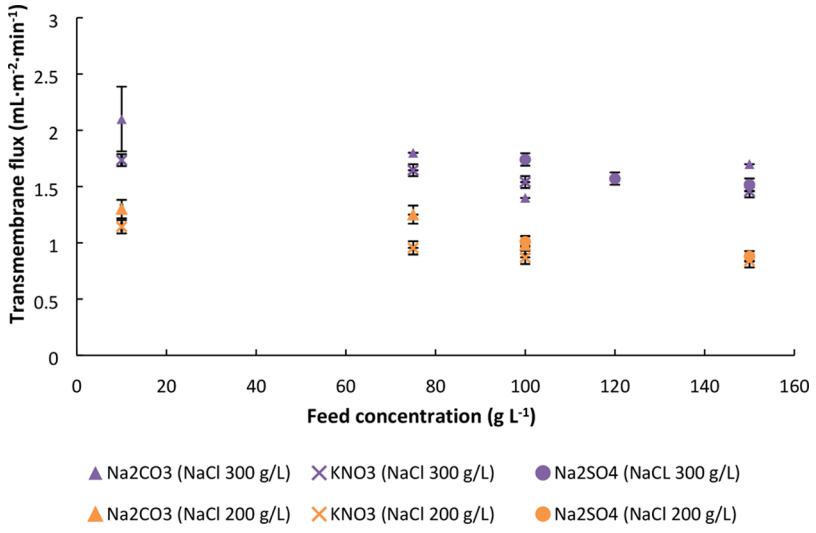

Figure 2. Transmembrane flux as a function of the feed concentration. Feed and NaCl flow rates are 300 and 450 mL min^{-1}, respectively. Values corresponding to 100 g L^{-1} Na_2CO_3 reprinted from Ruiz Salmón et al., (2017).[27] Room temperature.

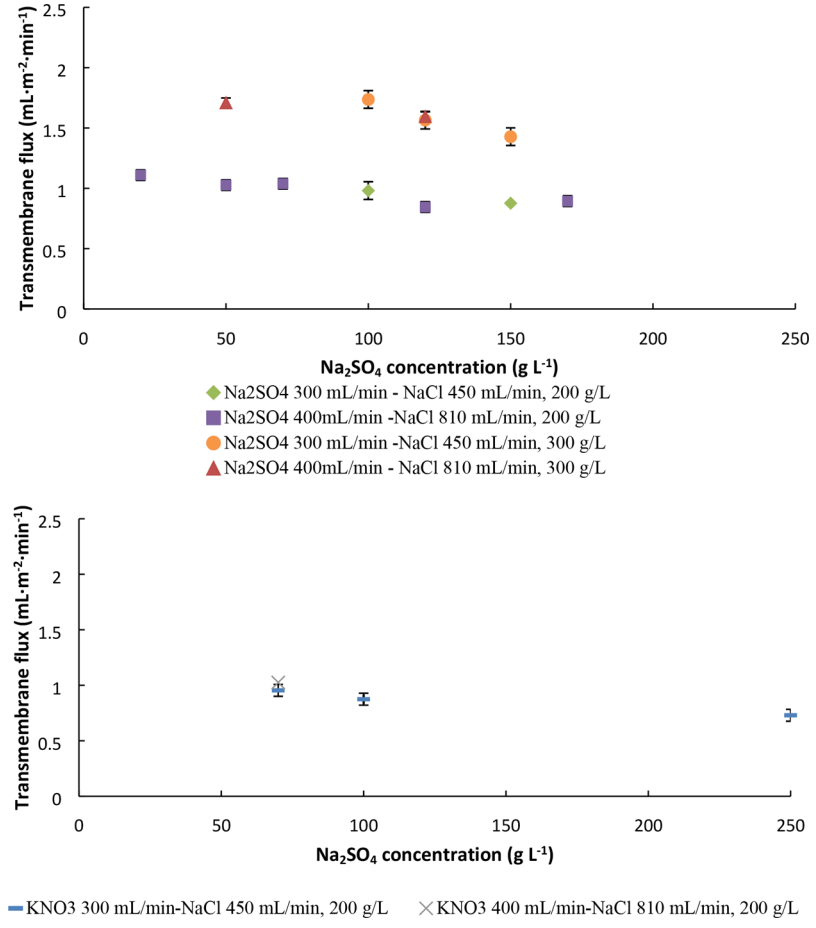

Figure 3. Transmembrane flux as a function of the feed concentration: (top) Na_2SO_4 and (bottom) KNO_3. Room temperature.

DOI: 10.1021/acs.cgd.8b00580
Cryst. Growth Des. 2018, 18, 7275−7285

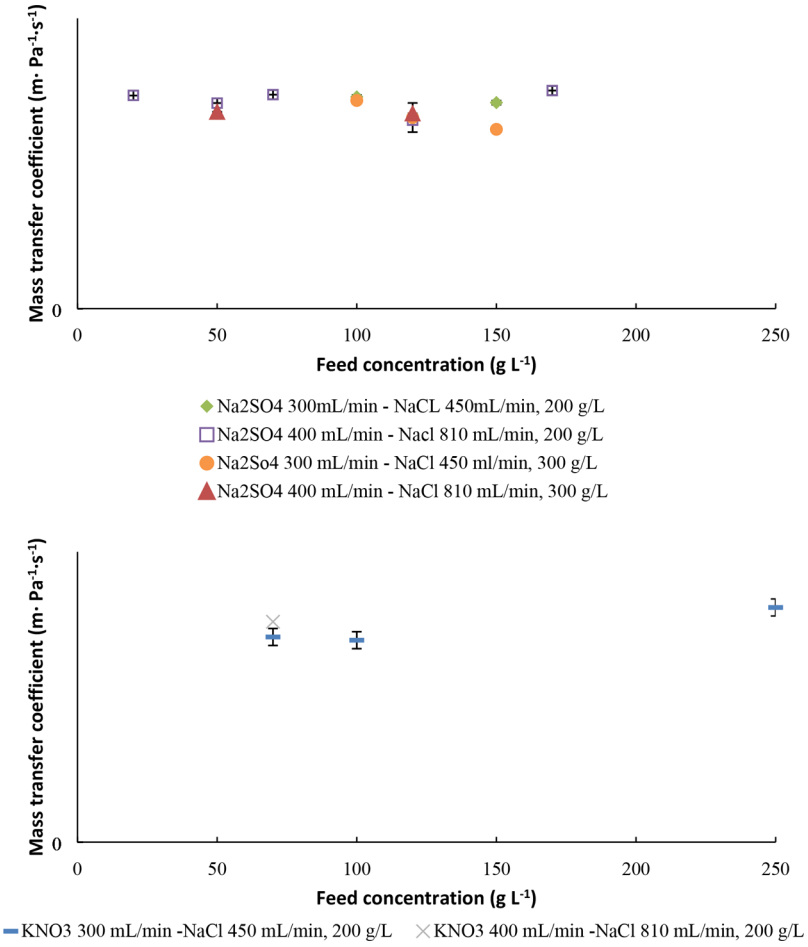

Figure 4. Mass transfer coefficient as a function of the feed concentration: (top) Na_2SO_4 and (bottom) KNO_3. Room temperature.

$$Ag^{+}_{(aq)} + SCN^{-}_{(aq)} \rightarrow AgSCN_{(s)} \quad \text{(R2)}$$

$$n_{Cl} = n_{AgNO_3} - n_{KSCN} \quad (4)$$

where n_{AgNO_3} is the number of moles of $AgNO_3$ added before the titration and n_{KSCN} is the quantity of KSCN added during the titration. To obtain the concentration of Cl^- that was previously in the solution, it is required to divide by the initial sample volume and take into account the potential dilution factor.

2.3.3. X-ray Diffraction. X-ray diffraction allows identifying the nature of the solid state. Here, the X-ray diffractometer produces an image (diffractogram) which depends on the nature of the crystalline phase.

A powder diffraction apparatus (Siemens D5000 equipped) was used to analyze the crystals with CuKα radiation λ = 1.5418 Å. The analyses were carried out at 40 kV and 40 mA, with a scan window of 2Θ value from 2 to 50°. The scan speed was 0.6 min^{-1}, and the pitch was 0.02°.

Clean samples of crystals were crushed and deposited on the wafer. Then, the analysis was started. The analysis of the results consists of a comparison of the spectra obtained for the crystals with the spectra from the literature.

2.3.4. Microscopy Tests. Crystals were examined by means of direct optical microscopy using a microscope Olympus AX70 Provis. A calibration was required to clarify the link pixel/distance.

3. RESULTS AND DISCUSSION

Four main variables, i.e., the concentration of feed and osmotic solutions, flow rates, impurities (traces of different salts, see Table 4) in the feed and number of membrane contactors (one or two in series), were studied to see their effect on the transmembrane flux, the mass transfer coefficient, and the crystallization process, according to the experimental conditions indicated in Table 2.

3.1. Influence of the Concentrations and Flow Rates on the Transmembrane Flux and Mass Transfer Coefficient. The experimental system indicated in Figure 1a was considered. Three inorganic salts, i.e., Na_2CO_3, Na_2SO_4, KNO_3, were used as feed simulating industrial wastewater. Feed concentration oscillated from 20 to 170 g L^{-1}, while osmotic solution varied from 200 to 300 g L^{-1}. The flow rates of the feed and osmotic solutions varied from 150 to 400 mL min^{-1} and from 300 to 810 mL min^{-1}, respectively.

Figure 2 shows the transmembrane flux as a function of the feed and osmotic solution concentration. The highest transmembrane flux is obtained when the highest concentration of osmotic solution is used (i.e., 300 g L^{-1} NaCl). On the other hand, the concentration of the feed solution has a slight effect on the flux. Thus, it is the variation of the concentration of the osmotic solution that led to a significant variation in the transmembrane flux. This trend can be explained in terms of the water activity. Figure S1 shows the values of water activity for the studied salts while varying the salt concentration. The water activity for NaCl varies significantly more with the concentration than the other salts. In other words, the driving force is more affected by a change in NaCl concentration than with the other salts. This means that the concentration of the osmotic solution has a large impact in the transmembrane flux.

DOI: 10.1021/acs.cgd.8b00580
Cryst. Growth Des. 2018, 18, 7275−7285

Regarding the kind of salt in the feed solution, no significant differences in transmembrane flux are observed (Figure 2). The transmembrane flux obtained is very similar, independently to the salt in the feed solution: Na_2CO_3, KNO_3, or Na_2SO_3. Again, the values of water activity in the feed solution are very similar for the concentration range studied for those salts (see Supporting Information). It can be concluded that the effect of feed concentration is negligible for the studied salts. On the contrary, NaCl concentration in the osmotic solution will have a large impact on the driving force and therefore on the final transmembrane flux.

Figures 3 and 4 present the fluxes and mass transfer coefficient against the concentrations of sodium sulfate and potassium nitrate, respectively, for several experimental conditions where feed concentration and both feed and osmotic flow rates were studied. Two combinations of feed/osmotic flow rates were employed: 300/450 and 400/810 mL min^{-1} for both salts. Two main conclusions may be inferred from the results: (1) the higher the osmotic concentration, the higher the transmembrane flux; (2) the variation of the flow rate hardly affects the final flux: the studied feed/osmotic solution velocities did not show any effect on both the transmembrane flux and the mass transfer coefficient of the sodium sulfate.

Regarding potassium nitrate, a slow decrease on the flux was observed when the feed concentration decreases. For the same feed and osmotic concentration, no influence of the flow rate was observed, with very similar results to those obtained with sodium sulfate. This is due to the water activities addressed in Figure S1 as previously stated, where the values for both salts are practically equal until 200 g L^{-1}.

Figure 4 displays the mass transfer coefficient for the same cases studied in Figure 3. This coefficient is the main parameter to evaluate the membrane performance since the effect of the driving force is eliminated, as indicated by eq 2. The constant value of the coefficients for all the experiments made for Na_2SO_4 ($4.77 \times 10^{-11} \pm 3.80 \times 10^{-12}$ m s^{-1} Pa^{-1}) and KNO_3 ($4.96 \times 10^{-11} \pm 5.32 \times 10^{-12}$ m s^{-1} Pa^{-1}) reveals that there were no phenomena of concentration polarization or wetting affecting the mass transfer, which makes the process less efficient than expected. Accordingly to eq 2, a constant value of the coefficients is always expected because the flux and the driving force are normally proportional. If this does not happen, a poorer yield of the membrane contactor would be produced, leading to a lower mass transfer coefficient. In this work, the presence of polarization is thus not observed. However, polarization was slightly noted in a previous work using osmotic membrane distillation for sodium carbonate crystallization with the same membrane contactor when feed flow rates lower than 50 mL min^{-1} were applied.[27] In that case, lower values of mass transfer coefficients were obtained when lower flow rates were used ($3.89 \times 10^{-11} \pm 7.28 \times 10^{-13}$ m s^{-1} Pa^{-1}). It was also observed that the mass transfer coefficients ($3.98 \times 10^{-11} \pm 1.48 \times 10^{-12}$ m s^{-1} Pa^{-1}) slightly decreased when the osmotic concentration passed from 100 g L^{-1} to 300 g L^{-1}, but it could not be explained by polarization phenomenon, and it was mentioned wetting of the pores as the possible cause.

3.2. Increasing the Membrane Area: Two Membrane Contactors in Series. The performance of two membrane contactors in series (Figure 1b) was evaluated in terms of transmembrane flux and overall mass transfer coefficient and compared with the results using one contactor. Figure 5 shows the comparison of transmembrane fluxes of the single setup and the two membranes in series. Results indicate that using two membrane contactors did not alter the normal trend of the system. The same transmembrane flux was obtained. This result validates one of the advantages of this kind of technology: the linear and easy scale-up. In this sense, previous works confirm this conclusion by comparing the mass transfer coefficients of different sizes of membrane contactors: minimodules[22,23,25,28] and extramodules.[27] In addition, the order of magnitude of the coefficients rounded the 10^{-12}–10^{-10} for similar technologies and applications.[17] Furthermore, the large area per volume, 3–40 times larger than conventional crystallization units,[29] and the small energy consumption, 5–36 times lower than traditional processes, such as multistage flash distillation or multieffect distillation,[17] make membrane crystallization as a powerful competitor.

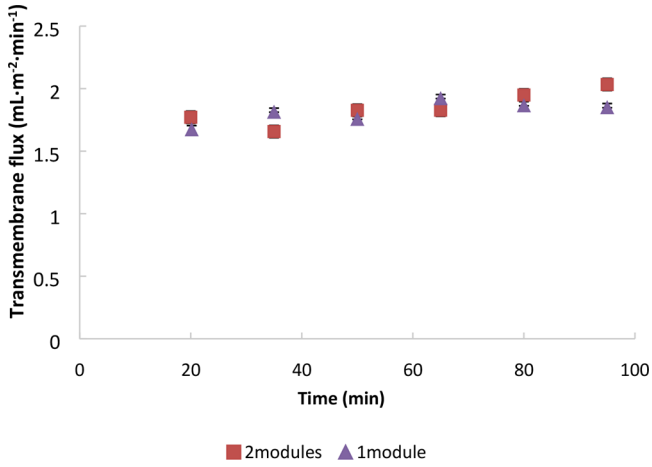

Figure 5. Transmembrane flux as a function of the number of membrane contactors. Na_2CO_3 concentration is 150 g L^{-1} and NaCl concentration is 300 g L^{-1}, feed and osmotic flow rates are 300 mL min^{-1} and 450 mL min^{-1}, respectively. Room temperature.

Using several modules in series instead of a larger contactor with the same membrane surface presents the advantage of using fresh osmotic solutions in each contactor with the desired concentration. Thus, depending on the final requirements of the wastewater treatment (different levels of concentration or crystallization), the driving forces can be perfectly controlled during all the process. In the studied case, the most logical configuration would be placing the highest osmotic concentration at the very beginning of the setup leading to remove the mayor part of water and, in the last stages, using osmotic solutions with low concentrations in order to avoid scaling in membranes.

3.3. Characteristics of Obtained Crystals. In addition to the evaluation of the effect of the operating conditions on the process performance, the characteristics of the crystals were also studied: morphology and purity.

3.3.1. Crystal Purity. Membrane crystallization experiments were made in the single setup using both pure solutions and mixtures of two or three salts at room temperature. Initial feed concentration of Na_2CO_3, Na_2SO_4, and KNO_3 was 200, 175, and 290 g L^{-1}, independently of the presence of impurities. These concentrations were chosen because they are close to the saturation (the solubilities of Na_2CO_3, Na_2SO_4, and KNO_3, which are 216 g L^{-1}, 192.3 g L^{-1}, and 316 g L^{-1}, respectively, at normal temperature and pressure), and then, the time of the

DOI: 10.1021/acs.cgd.8b00580
Cryst. Growth Des. 2018, 18, 7275–7285

experiments could be shorter. Composition of the mixtures are collected in Table 4.

The crystal purity was analyzed following different methods. First, total water content of the crystals was measured (Table 5) and compared with the theoretical values (Table 3). Thus, water fraction calculation revealed that sodium carbonate decahydrate ($Na_2CO_3 \cdot 10H_2O$) was obtained, which agrees with the typical diagram phase concentration−temperature.[30] Regarding the nitrates and sulfate, the applied operating conditions allowed producing sodium sulfate decahydrate ($Na_2SO_4 \cdot 10H_2O$) and potassium nitrate (KNO_3) during the experiments. Again, the binomial concentration−temperature diagrams of the sulfate[31] and the nitrate[32] corroborate the result. For the three salts, experimental total water fraction (TWF) was slightly higher than the theoretical ones. This may be because of the water uptake from the environment, leading to values of 6.25% and 4.55% for the nitrate and the carbonate, respectively.

Table 5. Total Water Fraction Obtained for Pure Solutions and Mixtures

crystal (+ impurities)	$TWF_{experimental}$ (wt %) according to eq 3
KNO_3	6 ± 3
Na_2CO_3	67 ± 3
Na_2SO_4	59 ± 1.5
Na_2CO_3 (+ KNO_3)	67 ± 4
Na_2CO_3 (+ KNO_3 + Na_2SO_4)	66 ± 1
Na_2SO_4 (+ KNO_3)	64 ± 4
Na_2SO_4 (+ KNO_3 + Na_2CO_3)	59.1 ± 0.3
KNO_3 (+ Na_2CO_3)	1 ± 1
KNO_3 (Na_2CO_3 + Na_2SO_4)	6 ± 5

Second, X-ray diffraction was carried out. The spectra of the crystals were compared with references (Figure 6). It can be seen that all peaks generated in the mixtures fit with the literature case. Similar conclusions were previously obtained, even with higher impurity concentrations at mother liquor[22] or in mixtures sodium carbonate-sodium sulfate.[24] The coincidence of the peaks reveals a high purity, even with the presence of impurities in the crystallizing solution, and, apparently, no cocrystallization occurred. This is due to the fact that membrane crystallization allows pure crystal production thanks to the low rate of evaporation and the low temperatures (room temperature was used in all the research).[22,33]

A second analysis, the Charpentier−Volhard's method, was applied in both solutions and crystals, in order to see if chloride ions passed from the permeate side to the feed solution and contaminate it. Three kinds of samples were studied (Table 6): pure solutions obtained using simple crystallization by evaporization; pure solutions used in membrane crystallization; and feed solutions with impurities. The first group of samples, i.e., crystals from evaporization and, therefore, without no contact with osmotic solution, were used as reference. It was observed, as expected, that the liquid phase was free of chlorides, and purity of the solute was 99.99%. In the second group, i.e., solutions after membrane crystallization, both liquid and rinsed crystals displayed a purity higher than

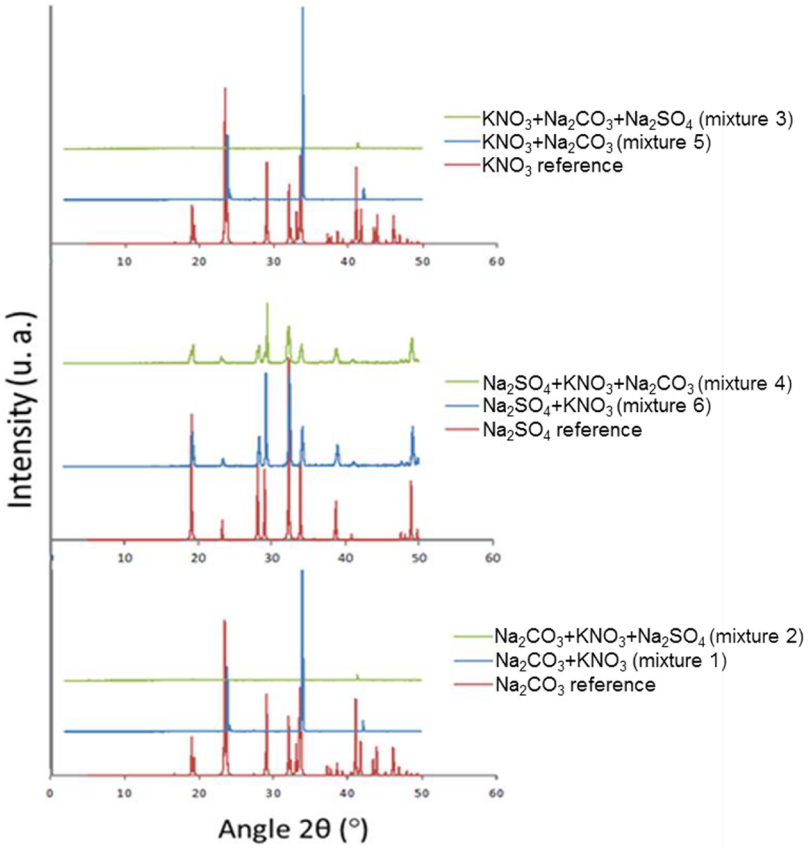

Figure 6. X-ray specters of salts. Green lines correspond to mixtures with two impurities; blue lines correspond to mixtures with one mixture and red lines correspond to literature reference of pure salts.

DOI: 10.1021/acs.cgd.8b00580
Cryst. Growth Des. 2018, 18, 7275−7285

Table 6. Amount of Cl^- in Liquid and Crystals

sample		Cl^- (g L^{-1}) liquid	Cl^- (g L^{-1}) rinsed crystals
feed solutions (crystallization by evaporization)	KNO_3	<0.005	
	Na_2CO_3	<0.005	
	Na_2SO_4	<0.005	
feed solutions (membrane cystallization)	KNO_3	0.51	<0.01
	Na_2CO_3	1.34	<0.01
	Na_2SO_4	0.50	<0.01
feed with impurities (membrane crystallization)	$Na_2CO_3 + KNO_3$	1.43	<0.01
	$Na_2CO_3 + KNO_3 + Na_2SO_4$	2.35	<0.01
	$Na_2SO_4 + KNO_3$	2.08	<0.01
	$Na_2SO_4 + KNO_3 + Na_2CO_3$	1.55	<0.01
	$KNO_3 + Na_2CO_3$	0.84	<0.01
	$KNO_3 + Na_2CO_3 + Na_2SO_4$	0.56	<0.01

99%, but a small presence of chlorides was detected. This indicates that a part of the osmotic solution got into the feed solution, which is not desirable. In this case, minor wetting occurs because Cl^- is detected in the feed solution, which is an undesired phenomenon, but there is not an important effect on the normal process (transmembrane fluxes) and the final purity of the crystal. It may be caused by the normal use of the membrane contactor for several years.

Finally, solutions with impurities showed similar results than the second group: pure crystals but solutions contaminated by chlorides.

3.3.2. Crystal Morphology. In crystalline materials, atoms are periodically arranged, but in amorphous materials atoms are randomly arranged. Thus, X-ray light incises in a crystal plane on atoms, then it scattered in a particular direction and gives a high intensity narrow peaks. In the case of amorphous materials, when X-ray light incises on atoms in a plane, it is scattered in random directions due to the random orientation of atoms, giving a broad peak or background hump.[34] Regarding the spectra of Figure 6, the structure of the salt reference (red patterns) is perfectly crystalline. On the other hand, for the salts analyzed (green and blue patterns), smaller and broad peaks can be appreciated and the presence of amorphous structures is revealed.

The three salts obtained by membrane crystallization are plotted in Figures 7, 8, and 9. Ordinary photo- and microscopy pictures of crystals from pure solutions (a), with one impurity (b) and with two impurities (c) are shown.

Pictures with subscript 1 in Figures 7–9 show that sodium carbonate and sodium sulfate crystals formed rounded agglomerates, while the small angled crystals of potassium nitrate appeared compacted in aggregation form where softer joins between the nuclei occur. Colorless crystals were obtained, indicating the presence of water molecules inside, as it has been previously stated.

Regarding the microscopy photos (suffix 2 in Figure 7–9), the characteristic shape of the crystal unit incrusted inside the whole agglomerates is indicated (pointed with arrows). Hexagonal shapes can be found in Figures $7a_2$ and $8a_2$ while the shape changes to the monoclinic and the triclinic shape when it exists in the presence of impurities.[22]

Figure 10 displays the nitrate crystals at different moments of the experimentation. Pictures $10a_1$ and $10a_2$ show the first big nuclei obtained and $10b_1$ and $10b_2$ the crystal piece a few hours after the process was finished. The difference of shape and size can be clearly seen. Here, heterogeneous nucleation, i.e., nuclei grow is assisted by suspended particles of a foreign substance or by solid objects such as the wall of the container,[18] took place in the set up. Membrane surface and the wall of the crystallizer used favored the heterogeneous nucleation, which is easier than the homogeneous nucleation (nuclei grow in the bulk solution). Primary nucleation took place first (no seeds were used) with a slow growth of the crystals up to reach a high supersaturation. Then, secondary nucleation started: solute in solution contacted with the surface of the initial nuclei. A rapid crystal grow was observed in the secondary nucleation against the primary one.[35] Again, small amorphous crystal units can be seen inside the clusters.

Although membrane crystallization succeeded, it was found that if no turbulences exist in the reservoir, larger sizes of carbonates are easily produced (Figure $10b_1$). For this reason, depending on the size that one is looking for, configuration (size, shape, etc.) of the crystallizer must be taken into account.

Finally, the efflorescence phenomenon, i.e., total or superficial conversion of a mass into powder caused by the loss of water, is addressed in Figure 11. This phenomenon describes a change of phase that occurs in both sulfate (Figure 11a) and carbonate (Figure 11b). Here, the water of the decahydrate sulfate and the decahydrate carbonate evaporates, and crystals change into the monohydrate and anhydrous form. This was

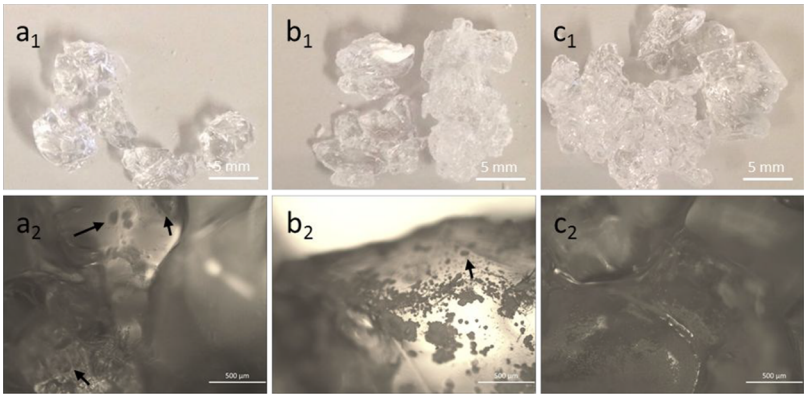

Figure 7. Na_2CO_3 crystals without impurities (a), with KNO_3 (b), and KNO_3 and Na_2SO_4 (c) impurities. Normal (1) and microscopy pictures (2).

DOI: 10.1021/acs.cgd.8b00580
Cryst. Growth Des. 2018, 18, 7275–7285

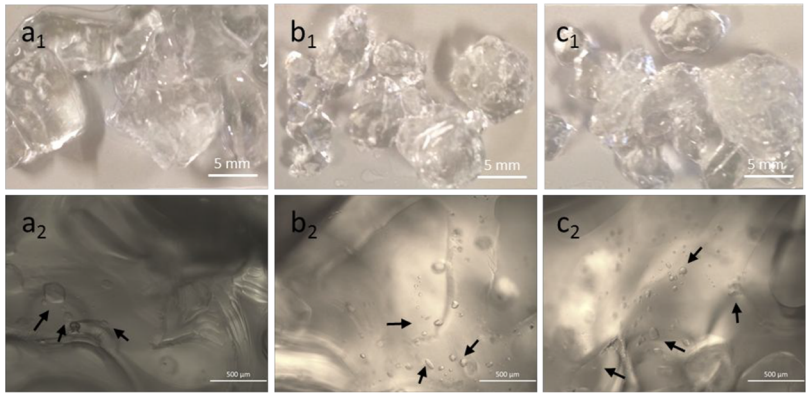

Figure 8. Na_2SO_4 crystals without impurities (a), with KNO_3 (b), and KNO_3 and Na_2CO_3 (c) impurities. Normal (1) and microscopy pictures (2).

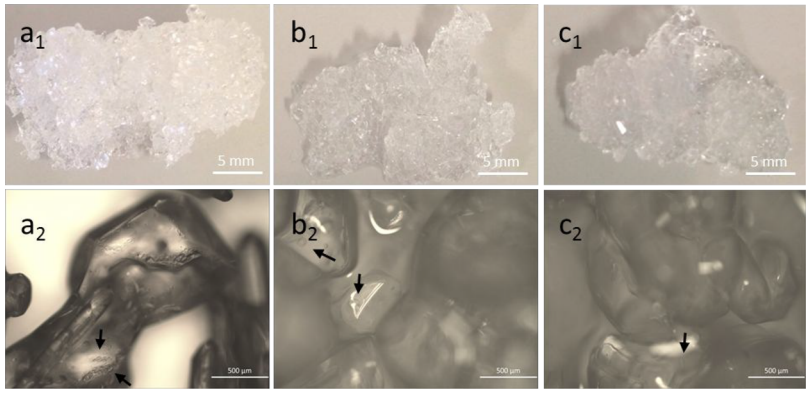

Figure 9. KNO_3 crystals without impurities (a), with Na_2CO_3 (b), and Na_2CO_3 and Na_2SO_4 (c) impurities. Normal (1) and microscopy pictures (2).

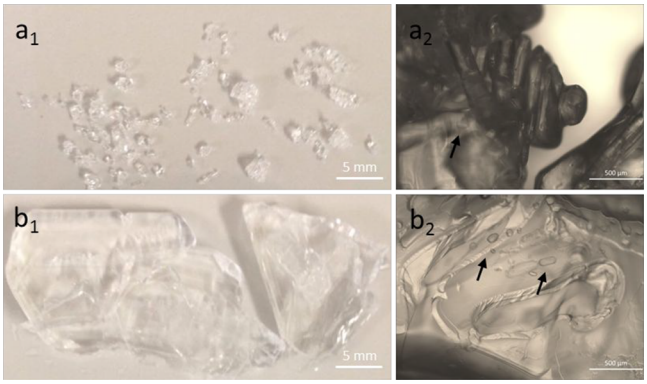

Figure 10. KNO_3 crystals without impurities: (a) at the beginning of the crystallization and (b) few hours later of finishing the experiment. Normal (1) and microscopy pictures (2).

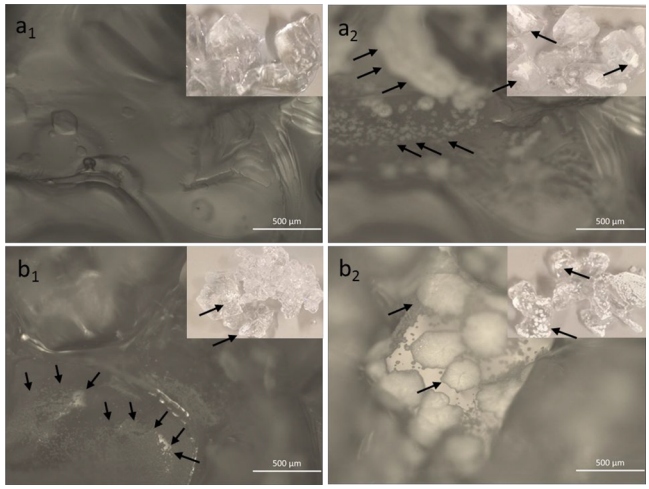

Figure 11. Na_2SO_4 without impurities (a) and Na_2CO_3 with impurities (b) crystals. White points correspond to a different phase of the crystals.

previously observed.[27] White surfaces (pointed with arrows) can be seen in both ordinary photo (top high of each picture) and the microscopy images. Efflorescence only takes place when some heat (even the sunlight) radiates the crystal. Figure 11a_1 was in the dark and Figure 11a_2 was put behind a light. Incipient efflorescence can be also seen in Figure 11b_1 (small white dots), and they become larger when the light time increases. In terms of industrial application, this phenomenon does not suppose a relevant problem if, for example, cement or ceramic production is the final objective, because water molecules inside the salts would not affect the process.

4. CONCLUSIONS

The crystallization of the inorganic salts (sodium sulfate, potassium nitrate, and sodium carbonate) was technically demonstrated using osmotic membrane distillation−crystallization. It was found that transmembrane fluxes were very influenced by the concentration of the osmotic solution (which generates the driving force in this process) and were not affected by the concentration of the feed side or the flow rate

DOI: 10.1021/acs.cgd.8b00580
Cryst. Growth Des. 2018, 18, 7275−7285

variation at both sides of the membrane. Furthermore, mass transfer coefficients were kept constant showing no problems of polarization of wetting. Using two membrane contactors in series kept the membrane performance.

Besides, potassium nitrate and decahydrate sodium carbonate and decahydrate sulfate crystals were produced without any effect of the impurities (small quantities of other salts in pure solutions) or the presence of chloride anions. Efflorescence phenomenon occurred when a soft heat source radiated the carbonates and the sulfates obtained, and, therefore, monohydrate and dehydrate forms of these crystals appeared on the surface.

■ ASSOCIATED CONTENT

Supporting Information

The Supporting Information is available free of charge on the ACS Publications website at DOI: 10.1021/acs.cgd.8b00580.

Water activities of pure solutions of Na_2CO_3, Na_2SO_4, KNO_3, and NaCl (Figure S1) were obtained by means of the sequence described by Sandler (2006).[36] Solubility curves of the three salts are plotted in Figures S2–S4 (PDF)

■ AUTHOR INFORMATION

Corresponding Author

*E-mail: israel.ruizsalmon@uclouvain.be.

ORCID

I. Ruiz Salmón: 0000-0001-7058-605X

Notes

The authors declare no competing financial interest.

■ ACKNOWLEDGMENTS

I.R.S. would like to acknowledge the help offered by Tom Leyssens in the evaluation of crystal morphology and the support of the research group Ecoefficient Processes for Sustainable Industrial Chemical and Biochemical Engineering in the Department of Materials and Process Engineering (IMAP) of the Institute of Mechanics, Materials and Civil Engineering (iMMC), at the Université Catholique de Louvain. The authors acknowledge the financial support by the Fonds spéciaux de recherche (FSR) of the Université Catholique de Louvain.

■ REFERENCES

(1) Qin, L.; Liu, Q.; Meng, Q.; Fan, Z.; He, J.; Liu, T.; Shen, C.; Zhang, G. Anoxic oscillating MBR for photosynthetic bacteria harvesting and high salinity wastewater treatment. *Bioresour. Technol.* **2017**, *224*, 69–77.

(2) Smith, V. H.; Tilman, G. D.; Nekola, J. C. Eutrophication: impacts of excess nutrient inputs on freshwater, marine, and terrestrial ecosystems. *Environ. Pollut.* **1999**, *100*, 179–196.

(3) Abrahams, M. V.; Kattenfeld, M. G. The role of turbidity as a constraint on predator-prey interactions in aquatic environments. *Behavior Ecol. Sociobiol.* **1997**, *40*, 169–174.

(4) Kim, Y. J.; Choi, J. H. Improvement of desalination efficiency in capacitive deionization using a carbon electrode coated with an ion-exchange polymer. *Water Res.* **2010**, *44*, 990–996.

(5) Jacob, C. Seawater desalination: boron removal by ion exchange technology. *Desalination* **2007**, *205*, 47–52.

(6) Lee, K. P.; Arnot, T. C.; Mattia, D. (2011). A review of reverse osmosis membrane materials for desalination—development to date and future potential. *J. Membr. Sci.* **2011**, *370*, 1–22.

(7) Hilal, N.; Al-Zoubi, H.; Darwish, N. A.; Mohamma, A. W.; Arabi, M. A. A comprehensive review of nanofiltration membranes: treatment, pretreatment, modelling, and atomic force microscopy. *Desalination* **2004**, *170*, 281–308.

(8) Chen, G.; Lu, Y.; Krantz, W. B.; Wang, R.; Fane, A. G. Optimization of operating conditions for a continuous membrane distillation crystallization process with zero salty water discharge. *J. Membr. Sci.* **2014**, *450*, 1–11.

(9) Hermassi, M.; Valderrama, C.; Dosta, J.; Cortina, J. L.; Batis, N. H. Evaluation of hydroxyapatite crystallization in a batch reactor for the valorization of alkaline phosphate concentrates from wastewater treatment plants using calcium chloride. *Chem. Eng. J.* **2015**, *267*, 142–152.

(10) Astarita, G. Absorption of carbon dioxide into alkaline solutions in packed towers. *Ind. Eng. Chem. Fundam.* **1963**, *2*, 294–297.

(11) Chu, H.; Chien, T. W.; Li, S. Y. Simultaneous absorption of SO_2 and NO from flue gas with KMnO4/NaOH solutions. *Sci. Total Environ.* **2001**, *275*, 127–135.

(12) Pradhan, M. P.; Joshi, J. B. Absorption of NOx gases in aqueous NaOH solutions: selectivity and optimization. *AIChE J.* **1999**, *45*, 38–50.

(13) Muller, H. Sulfur dioxide. In Ullmanns Encyclopedia of Industrial Chemistry, 2005.

(14) Quist-Jensen, C. A.; Macedonio, F.; Horbez, D.; Drioli, E. Reclamation of sodium sulfate from industrial wastewater by using membrane distillation and membrane crystallization. *Desalination* **2017**, *401*, 112–119.

(15) Ulrich, J.; Jones, M. J. Industrial crystallization: developments in research and technology. *Chem. Eng. Res. Des.* **2004**, *82*, 1567–1570.

(16) Chabanon, E.; Mangin, D.; Charcosset, C. Membranes and crystallization processes: state of the art and prospects. *J. Membr. Sci.* **2016**, *509*, 57–67.

(17) Ruiz Salmón, I.; Luis, P. Membrane crystallization via membrane distillation. *Chem. Eng. Process.* **2018**, *123*, 258–271.

(18) Drioli, E.; Criscuoli, A.; Curcio, E. *Membrane Contactors: Fundamentals, Applications and Potentialities*; Elsevier: The Netherlands, 2011.

(19) Ye, W.; Wu, J.; Ye, F.; Zeng, H.; Tran, A. T.; Lin, J.; Luis, P.; Van der Bruggen, B. Potential of osmotic membrane crystallization using dense membranes for Na_2CO_3 production in a CO_2 capture scenario. *Cryst. Growth Des.* **2015**, *15*, 695–705.

(20) Lawson, K. W.; Lloyd, D. R. Membrane distillation. *J. Membr. Sci.* **1997**, *124*, 1–25.

(21) Lawson, K. W.; Lloyd, D. R. Membrane distillation. II. Direct contact MD. *J. Membr. Sci.* **1996**, *120*, 123–133.

(22) Ye, W.; Lin, J.; Shen, J.; Luis, P.; Van der Bruggen, B. Membrane crystallization of sodium carbonate for carbon dioxide recovery: effect of impurities on the crystal morphology. *Cryst. Growth Des.* **2013**, *13*, 2362–2372.

(23) Li, W.; Van der Bruggen, B.; Luis, P. Integration of reverse osmosis and membrane crystallization for sodium sulphate recovery. *Chem. Eng. Process.* **2014**, *85*, 57–68.

(24) Li, W.; Van der Bruggen, B.; Luis, P. Recovery of Na_2CO_3 and Na_2SO_4 from mixed solutions by membrane crystallization. *Chem. Eng. Res. Des.* **2016**, *106*, 315–326.

(25) Luis, P.; Van Aubel, D.; Van der Bruggen, B. Technical viability and exergy analysis of membrane crystallization: Closing the loop of CO_2 sequestration. *Int. J. Greenhouse Gas Control* **2013**, *12*, 450–459.

(26) Luis, P. *Fundamental Modelling of Membrane Systems*; Elsevier, 2018.

(27) Ruiz Salmón, I.; Janssens, R.; Luis, P. Membrane crystallization of sodium carbonate in CO_2 capture scenario: mass and heat transfer study. *Sep. Purif. Technol.* **2017**, *176*, 173–183.

(28) Brito Martínez, M.; Jullok, N.; Negrín, Z. R.; Van der Bruggen, B.; Luis, P. Membrane crystallization for the recovery of a pharmaceutical compound from waste streams. *Chem. Eng. Res. Des.* **2014**, *92*, 264–272.

(29) Noble, R. D.; Stern, S. A., Eds. *Membrane Separations Technology: Principles and Applications*; Elsevier: The Netherlands, 1995.
(30) Kobe, K. A.; Sheehy, T. M. Thermochemistry of sodium carbonate and its solutions. *Ind. Eng. Chem.* **1948**, *40*, 99−102.
(31) Rodríguez-Navarro, C.; Doehne, E.; Sebastian, E. How does sodium sulfate crystallize? Implications for the decay and testing of building materials. *Cem. Concr. Res.* **2000**, *30*, 1527−1534.
(32) Laval, P.; Giroux, C.; Leng, J.; Salmon, J. B. Microfluidic screening of potassium nitrate polymorphism. *J. Cryst. Growth* **2008**, *310*, 3121−3124.
(33) Bialik, M. A.; Theliander, H.; Sedin, P.; Verrill, C. L.; DeMartini, N. *Ind. Eng. Chem. Res.* **2008**, *47*, 3233−3238.
(34) Katz, L. X-ray diffraction in crystals, imperfect crystals, and amorphous bodies (Guinier, A.). *J. Chem. Educ.* **1964**, *41*, 292.
(35) Drioli, E.; Curcio, E.; Criscuoli, A.; Di Profio, G. Integrated system for recovery of $CaCO_3$, NaCl and $MgSO_4{\cdot}7H_2O$ from nanofiltration retentate. *J. Membr. Sci.* **2004**, *239*, 27−38.
(36) Sandler, S. I. *Chemical, Biochemical, and Engineering Thermodynamics*; John Wiley & Sons: USA, 2006.

DOI: 10.1021/acs.cgd.8b00580
Cryst. Growth Des. 2018, 18, 7275−7285